

Computer simulations of electrorheological fluids in the dipole-induced dipole model

Y. L. Siu, Jones T. K. Wan and K. W. Yu

Department of Physics, The Chinese University of Hong Kong,

Shatin, New Territories, Hong Kong, China

Abstract

We have employed the multiple image method to compute the interparticle force for a polydisperse electrorheological (ER) fluid in which the suspended particles can have various sizes and different permittivities. The point-dipole (PD) approximation being routinely adopted in computer simulation of ER fluids is shown to err considerably when the particles approach and finally touch due to multipolar interactions. The PD approximation becomes even worse when the dielectric contrast between the particles and the host medium is large. From the results, we show that the dipole-induced-dipole (DID) model yields very good agreements with the multiple image results for a wide range of dielectric contrasts and polydispersity. As an illustration, we have employed the DID model to simulate the athermal aggregation of particles in ER fluids both in uniaxial and rotating fields. We find that the aggregation time is significantly reduced. The DID model accounts for multipolar interaction partially and is simple to use in computer simulation of ER fluids.

PACS Number(s): 83.80.Gv, 82.70.Dd, 41.20.-q

Typeset using REVTeX

I. INTRODUCTION

The prediction of the yield stress for electrorheological (ER) fluids is the main concern in theoretical investigations of ER fluids. Early studies failed to derive the experimental yield stress data [1] because these studies were almost based on a point-dipole approximation [2,3]. The point-dipole approximation is routinely adopted in computer simulation because it is simple and easy to use. Since many-body and multipolar interactions between particles have been neglected, the strength of ER effects predicted by this model is of an order lower than the experimental results. Hence, substantial effort has been made to sort out more accurate models.

Klingenberg and coworkers developed empirical force expression from numerical solution of Laplace's equation [4]. Davis used the finite-element method [5]. Clercx and Bossis developed a full multipolar treatment to account for multipolar polarizability of spheres up to 1,000 multipolar orders [6]. Yu and coworkers developed an integral equation method which avoids the match of complicated boundary conditions on each interface of the particles and is applicable to nonspherical particles and multimedia [7]. Although the above methods are accurate, they are relatively complicated to use in dynamic simulation of ER fluids. Alternative models have been developed to circumvent the problem: the coupled-dipole model [8] and the dipole-induced-dipole model [9], which take care of mutual polarization effects when the particles approach and finally touch.

The DID model accounts for multipolar interactions partially and is simple to use in computer simulation of ER fluids [9]. As an illustration, we employed the DID model to simulate the athermal aggregation of particles in ER fluids both in uniaxial and rotating fields. We find that the aggregation time is significantly reduced. In the next section, we review the multiple image method and establish the dipole-induced dipole (DID) model. In section III, we apply the DID model to the computer simulation of ER fluids in a uniaxial field. In section IV, we extend the simulation to athermal aggregation in rotating fields. Discussion on our results will be given.

II. IMPROVED MULTIPLE IMAGE METHOD

Here we briefly review the multiple images method [9] and extend the method slightly to handle different dielectric constants. Consider a pair of dielectric spheres, of radii a and b , dielectric constants ϵ_1 and ϵ'_1 respectively, separated by a distance r . The spheres are embedded in a host medium of dielectric constant ϵ_2 . Upon the application of an electric field \mathbf{E}_0 , the induced dipole moment inside the spheres are respectively given by (SI units):

$$p_{a0} = 4\pi\epsilon_0\epsilon_2\beta E_0 a^3, \quad p_{b0} = 4\pi\epsilon_0\epsilon_2\beta' E_0 b^3, \quad (1)$$

where the dipolar factors β, β' are given by:

$$\beta = \frac{\epsilon_1 - \epsilon_2}{\epsilon_1 + 2\epsilon_2}, \quad \beta' = \frac{\epsilon'_1 - \epsilon_2}{\epsilon'_1 + 2\epsilon_2}. \quad (2)$$

From the multiple image method [9], the total dipole moment inside sphere a is:

$$p_{aT} = (\sinh \alpha)^3 \sum_{n=1}^{\infty} \left[\frac{p_{a0} b^3 (-\beta)^{n-1} (-\beta')^{n-1}}{(b \sinh n\alpha + a \sinh(n-1)\alpha)^3} + \frac{p_{b0} a^3 (-\beta)^n (-\beta')^{n-1}}{(r \sinh n\alpha)^3} \right], \quad (3)$$

$$p_{aL} = (\sinh \alpha)^3 \sum_{n=1}^{\infty} \left[\frac{p_{a0} b^3 (2\beta)^{n-1} (2\beta')^{n-1}}{(b \sinh n\alpha + a \sinh(n-1)\alpha)^3} + \frac{p_{b0} a^3 (2\beta)^n (2\beta')^{n-1}}{(r \sinh n\alpha)^3} \right], \quad (4)$$

where the subscripts T (L) denote a transverse (longitudinal) field, i.e., the applied field is perpendicular (parallel) to the line joining the centers of the spheres. Similar expressions for the total dipole moment inside sphere b can be obtained by interchanging a and b , as well as β and β' . The parameter α satisfies:

$$\cosh \alpha = \frac{r^2 - a^2 - b^2}{2ab}.$$

In Ref. [9], we checked the validity of these expressions by comparing with the integral equation method. We showed that these expressions are valid at high contrast. Our improved expressions will be shown to be good at low contrast as well (see below).

The force between the spheres is given by [10]:

$$F_T = \frac{E_0}{2} \frac{\partial}{\partial r} (p_{aT} + p_{bT}), \quad F_L = \frac{E_0}{2} \frac{\partial}{\partial r} (p_{aL} + p_{bL}). \quad (5)$$

For monodisperse ER fluids ($a = b$, $\beta = \beta'$ and $p_a = p_b = p_0$), Klingenberg defined an empirical force expression [4]:

$$\frac{\mathbf{F}}{F_{PD}} = (2K_{\parallel} \cos^2 \theta - K_{\perp} \sin^2 \theta) \hat{\mathbf{r}} + K_{\Gamma} \sin 2\theta \hat{\boldsymbol{\theta}}, \quad (6)$$

being normalized to the point-dipole force $F_{PD} = -3p_0^2/r^4$, where K_{\parallel} , K_{\perp} and K_{Γ} (all tending to unity at large separations) are three force functions being determined from the numerical solution of Laplace's equation. The Klingenberg's force functions can be shown to relate to our multiple image moments as follow (here $a = b$, $\beta = \beta'$ and $p_a = p_b$):

$$K_{\parallel} = \frac{1}{2} \frac{\partial \tilde{p}_L}{\partial r}, \quad K_{\perp} = -\frac{\partial \tilde{p}_T}{\partial r}, \quad K_{\Gamma} = \frac{1}{r} (\tilde{p}_T - \tilde{p}_L), \quad (7)$$

where $\tilde{p}_L = p_L/F_{PD}E_0$ and $\tilde{p}_T = p_T/F_{PD}E_0$ are the reduced multiple image moments of each sphere. We computed the numerical values of these force functions separately by the approximant of Table I of the second reference of Ref. [4] and by Eq.(7).

In Fig.1, we plot the multiple image results and the Klingenberg's empirical expressions. We show results for the perfectly conducting limit ($\beta = 1$) only. For convenience, we define the reduced separation $\sigma = r/(a + b)$. For reduced separation $\sigma > 1.1$, simple analytic expressions were adopted by Klingenberg. As evident from Fig.1, the agreement with the multiple image results is impressive at large reduced separation $\sigma > 1.5$, for all three empirical force functions. However, significant deviations occur for $\sigma < 1.5$, especially for K_{\parallel} . For $\sigma \leq 1.1$, alternative empirical expressions were adopted by Klingenberg. For K_{\perp} , the agreement is impressive, although there are deviations for the other two functions. From the comparison, we would say that reasonable agreements have been obtained. Thus, we are confident that the multiple image expressions give reliable results.

The analytic multiple image results can be used to compare among the various models according to how many terms are retained in the multiple image expressions: (a) point-dipole (PD) model: $n = 1$ term only, (b) dipole-induced-dipole (DID) model: $n = 1$ to $n = 2$ terms only, and (c) multipole-induced-dipole (MID) model: $n = 1$ to $n = \infty$ terms.

In a previous work [9], we examine the case of different size but equal dielectric constant ($\beta = \beta'$) only. Here we focus on the case $a = b$ and study the effect of different dielectric

constants. In Fig.2, we plot the interparticle force in the longitudinal field case against the reduced separation σ between the spheres for (a) $\beta = 9/11$ ($\epsilon_1/\epsilon_2 = 10$) and (b) $\beta = 1/3$ ($\epsilon_1/\epsilon_2 = 2$) and various β'/β ratios. At low contrast, the DID model almost coincides with the MID results. In contrast, the PD model exhibits significant deviations. It is evident that the DID model generally gives better results than PD for all polydispersity.

III. COMPUTER SIMULATION IN THE DIPOLE-INDUCED-DIPOLE MODEL

The multiple image expressions [Eqs.(3)–(4)] allows us to calculate the correction factor defined as the ratio between the DID and PD forces:

$$\frac{F_{DID}^{(\perp)}}{F_{PD}^{(\perp)}} = 1 - \frac{\beta a^3 r^5}{(r^2 - b^2)^4} - \frac{\beta' b^3 r^5}{(r^2 - a^2)^4} + \frac{\beta \beta' a^3 b^3 (3r^2 - a^2 - b^2)}{(r^2 - a^2 - b^2)^4}, \quad (8)$$

$$\frac{F_{DID}^{(\parallel)}}{F_{PD}^{(\parallel)}} = 1 + \frac{2\beta a^3 r^5}{(r^2 - b^2)^4} + \frac{2\beta' b^3 r^5}{(r^2 - a^2)^4} + \frac{4\beta \beta' a^3 b^3 (3r^2 - a^2 - b^2)}{(r^2 - a^2 - b^2)^4}, \quad (9)$$

$$\frac{F_{DID}^{(\Gamma)}}{F_{PD}^{(\Gamma)}} = 1 + \frac{\beta a^3 r^3}{2(r^2 - b^2)^3} + \frac{\beta' b^3 r^3}{2(r^2 - a^2)^3} + \frac{3\beta \beta' a^3 b^3}{(r^2 - a^2 - b^2)^3}, \quad (10)$$

where $F_{PD}^{(\perp)} = 3p_{a0}p_{b0}/r^4$, $F_{PD}^{(\parallel)} = -6p_{a0}p_{b0}/r^4$ and $F_{PD}^{(\Gamma)} = -3p_{a0}p_{b0}/r^4$ are the point-dipole forces for the transverse, longitudinal and Γ cases respectively. These correction factors can be readily calculated in computer simulation of polydisperse ER fluids. The results show that the DID force deviates significantly from the PD force at high contrast when β and β' approach unity. The dipole induced interaction will generally decrease (increase) the magnitude of the transverse (longitudinal) interparticle force with respect to the point-dipole limit.

For simplicity, we consider the case of two equal spheres of radius a , initially at rest and at a separation d_0 . An electric field is applied along the line joining the centers of the sphere. The equation of motion is given by:

$$\frac{dz}{dt} = F_{\parallel}(2z), \quad (11)$$

where z is the displacement of one sphere from the center of mass. The separation between the two spheres is thus $d = 2z$ and the initial condition is $d = d_0$ at $t = 0$. Eq.(11)

is a dimensionless equation. We have chosen the following natural scales to define the dimensionless variables:

$$\text{length} \sim a, \quad \text{time} = t_0 \sim \frac{6\pi\eta_c a^2}{F_0}, \quad \text{force} = F_0 \sim \frac{\epsilon_0 \epsilon_2^2 a^2 E_0^2}{4\pi},$$

where E_0 is the field strength, m is the mass, η_c is the coefficient of viscosity. Using typical parameters, we find t_0 is of the order milliseconds. We have followed Klingenberg [2,3] to ignore the inertial effect, captured by the parameter G .

$$G = \frac{\epsilon_0 m \epsilon_2^2 E_0^2}{144\pi^3 \eta_c^2 a},$$

The neglect of G can be justified as follows. For values common to ER suspension: $\eta_c \approx 0.1$ Pa s, $m \approx 8 \times 10^{-13}$ kg, $a \approx 5 \times 10^{-6}$ m [2], The inertial term G is of the order 10^{-8} . We also neglect the thermal motion of the particles which is a valid assumption at high fields. We should remark that the initial separation d_0 is related to the volume fraction ϕ , defined as the ratio of the volume of the sphere to that of the cube which contains the sphere [3], i.e. $\phi = V_{\text{sphere}}/V_{\text{cube}}$, and

$$\frac{d_0}{2a} = \left(\frac{\pi}{6\phi} \right)^{1/3}.$$

For the PD approximation, Eq.(11) admits an analytic solution:

$$z = \left[\left(\frac{d_0}{2} \right)^5 - \frac{15p_0^2 t}{8} \right]^{1/5}. \quad (12)$$

We integrate the equation of motion by the 4th order Runge-Kutta algorithm, with time steps $\delta t = 0.01$ and 0.001 for small and large volume fractions respectively. In Fig.3(a), we plot the displacement d/a versus time graph for the PD case and find excellent agreement between analytic and numerical results.

For the DID model, we have to integrate the equation of motion numerically. In Fig.4, we plot the displacement d/a versus time graph for the aggregation of two spheres in uniaxial fields. At small volume fractions, i.e., when the initial separation is large, the time for aggregation is large and the DID results deviate slightly from the PD results. However, at

large volume fractions, the DID results are significantly smaller than the PD calculations. The effect becomes even more pronounced at large β .

In Fig.5(a), we plot the ratio of aggregation time of the DID to PD cases. The results showed clearly that the aggregation time has been significantly reduced when mutual polarization effects are considered. The reduction in aggregation time becomes even pronounced for small initial separations.

IV. ATHERMAL AGGREGATION IN THE ROTATING FIELD

Recently, Martin and coworkers [11] demonstrated athermal aggregation with the rotating field. When a rotating field is applied in the x - y plane at a sufficiently high frequency that particles do not move much in one period, an average attractive dipolar interaction is created. The result of this is the formation of plates in the x - y plane. Consider a rotating field applied in the x - y plane: $E_x = E_0 \cos \omega t$, $E_y = E_0 \sin \omega t$. The dimensionless equation of motion for the two sphere case becomes:

$$\frac{dx}{dt} = F_{\parallel} \cos^2 \omega t + F_{\perp} \sin^2 \omega t, \quad \frac{dy}{dt} = -F_{\Gamma} \sin 2\omega t, \quad (13)$$

where (x, y) is the displacement of one sphere from the center of mass. For large ω , we may safely neglect the y component of the motion. In the PD approximation, $F_{\parallel} = -6p_0^2/r^4$ and $F_{\perp} = 3p_0^2/r^4$, we find the analytic result:

$$x = \left[\left(\frac{d_0}{2} \right)^5 - \frac{15p_0^2}{64\omega} (2\omega t + 3 \sin 2\omega t) \right]^{1/5}. \quad (14)$$

The separation between the two spheres is just $d = 2x$, with the initial separation $d = d_0$ at $t = 0$. In the rotating field case, we also integrate the equation of motion by the 4th order Runge-Kutta algorithm, but with $\delta t = 1/(4\omega)$ and $1/(40\omega)$ as the time steps. Note that $\delta t = 1/(4\omega)$ should be the largest time step which can be used because we must at least go through a cycle consisting of the transverse and longitudinal field cases. The oscillating effect of a rotating field is less observable when the time step is smaller than this maximum value.

In Fig.3(b), we plot the displacement versus time graph for the PD case in rotating field and find an excellent agreement between analytic and numerical results. It is evident that the aggregation time is 4 times of that of the uniaxial field case. In fact, Eq.(14) reduces to Eq.(12) as $\omega \rightarrow 0$. However, at large ω , Eq.(14) becomes:

$$x = \left[\left(\frac{d_0}{2} \right)^5 - \frac{15p_0^2 t}{32} \right]^{1/5}.$$

That is, in the PD approximation, the time average force becomes 1/4 of that of the uniaxial field case. It is because the two dipole moments spend equal times in the transverse and longitudinal orientations, while $F_{\parallel} = -2F_{\perp}$ in the PD case, leading to an overall attractive force that is 1/4 of the force of the uniaxial field case. When the multiple image force is included, we expect that the magnitude of F_{\parallel} increases while that of F_{\perp} decreases and we expect an even larger attractive force when the spheres approach. In this case, the aggregation time must be reduced even more significantly.

In Fig.5(b), we plot the ratio of aggregation time of the DID to PD cases for $\beta = 1$ and several ω . The $\omega = 0$ curve is just for the uniaxial field case. The results showed clearly that the aggregation time has been significantly reduced when mutual polarization effects are considered. The reduction in aggregation time becomes even pronounced for small initial separations. It is observed that fluctuations exist when the initial separation between the spheres is $2.4a$ or less. It is because the motion is sensitive to the initial orientation of the dipoles when the spheres are too close.

Similarly, we consider the aggregations of 3 and 4 equal spheres, arranged in a chain, an equilateral triangle and a square. For a chain of 3 spheres in a rotating field, the central sphere does not move, while the two spheres at both ends move towards the central sphere. For 3 spheres in an equilateral triangle, the center of mass (CM) will not move while each sphere moves towards the CM, subject to the force of the other two spheres. The same situation occurs for 4 spheres in a square, in which each sphere moves towards the CM, subject to the force of the other 3 spheres.

In the PD approximation, we report the analytic results as follows. For 3 spheres in a

chain,

$$x = \left[d_0^5 - \frac{255p_0^2}{64\omega} (2\omega t + 3 \sin 2\omega t) \right]^{1/5}. \quad (15)$$

For 3 spheres in an equilateral triangle,

$$x = \left[\left(\frac{d_0}{\sqrt{3}} \right)^5 - \frac{5p_0^2}{8\sqrt{3}\omega} (4\omega t - \sin 2\omega t) \right]^{1/5}. \quad (16)$$

For 4 spheres in a square,

$$x = \left[\left(\frac{d_0}{\sqrt{2}} \right)^5 - \frac{15p_0^2}{8\omega} \left(\frac{4\sqrt{2} + 1}{4} \omega t - \frac{8\sqrt{2} - 3}{8} \sin 2\omega t \right) \right]^{1/5}. \quad (17)$$

In each of the above cases, x is the distance of one sphere from the center of mass. In the case of 3 spheres in a chain, the separation between the spheres is same as $d = x$. In the case of 3 spheres in an equilateral triangle, the separation between spheres is $d = \sqrt{3}x$. In the case of 4 spheres in a square, the separation between spheres is $d = \sqrt{2}x$. Again, we integrate the equation of motion by the 4th order Runge-Kutta algorithm. We find excellent agreements between the analytic and numerical results (not shown here).

It has been found that the displacement in the y -direction is about 0.5% for $\omega = 5$ and a larger ω has been used in the simulation. On the other hand, it is time consuming for simulations with $\omega > 20$. It is evident from the displacement-time graph that the results are correct. In Fig.6, the oscillation amplitude is reduced when the rotating frequency increases in the simulation. This is consistent with the assumption made in our analytic expressions. In Fig.7, it is observed that fluctuations exist when the initial separation between the spheres is $2.4a$ or less in all three graphs. Again, it is because the motion is sensitive to the orientation of the dipoles when the spheres are close. From the simulation, the reduction effects become even pronounced for the rotating electric field case than the uniaxial field case.

DISCUSSION AND CONCLUSION

Here a few comments on our results are in order. In this work, we studied the aggregation time for several particles. We should also examine the morphology of aggregation, due to

multiple image forces. In this connection, we can also examine the structural transformation by applying the uniaxial and rotating fields simultaneously [12].

We have done simulation in the monodisperse case. Real ER fluids must be polydisperse in nature: the suspending particles can have various sizes or different permittivities. Polydisperse electrorheological (ER) fluids have attracted considerable interest recently because the size distribution and dielectric properties of the suspending particles can have significant impact on the ER response [13]. We should extend the simulation to polydisperse case by using the DID model.

In summary, we have used the multiple image to compute the interparticle force for a polydisperse electrorheological fluid. We apply the formalism to a pair of spheres of different dielectric constants and calculate the force as a function of the separation. The results show that the point-dipole approximation is oversimplified. It errs considerably because many-body and multipolar interactions are ignored. The dipole-induced-dipole model accounts for multipolar interactions partially and yields overall satisfactory results in computer simulation of ER fluids while it is easy to use.

ACKNOWLEDGMENTS

This work was supported by the Research Grants Council of the Hong Kong SAR Government under grant CUHK4284/00P.

REFERENCES

- [1] P. M. Adriani and A. P. Gast, *Phys. Fluids* **31**, 2757 (1988).
- [2] D. J. Klingenberg, F. van Swol and C. F. Zukoski, *J. Chem. Phys.* **91**, 7888 (1989).
- [3] D. J. Klingenberg, F. van Swol and C. F. Zukoski, *J. Chem. Phys.* **94**, 6160 (1991).
- [4] D. J. Klingenberg and C. F. Zukoski, *Langmuir* **6** 15 (1990); D. J. Klingenberg, F. van Swol and C. F. Zukoski, *J. Chem. Phys.* **94**, 6170 (1991).
- [5] L. C. Davis, *Appl. Phys. Lett.* **60**, 319 (1992).
- [6] H. J. H. Clercx and G. Bossis, *Phys. Rev. E* **48**, 2721 (1993).
- [7] K. W. Yu, Hong Sun and Jones T. K. Wan, in *Proceedings of the 5th International Conference on Electrical Transport and Optical Properties of Inhomogeneous Media*, *Physica B* **279**, 78 (2000).
- [8] Z. W. Wang, Z. F. Lin and R. B. Tao, *Int. J. Mod. Phys.* **10**, 1153 (1996).
- [9] K. W. Yu and Jones T. K. Wan, in *Proceedings of the 9th International Conference on Discrete Simulation of Fluid Dynamics*, *Comput. Phys. Comm.* **129**, 177 (2000).
- [10] J. D. Jackson, *Classical Electrodynamics* (Wiley, New York 1975).
- [11] J. E. Martin, R. A. Anderson and C. P. Tigges, *J. Chem. Phys.* **108**, 3765 (1998); **108**, 7887 (1998).
- [12] C. K. Lo and K. W. Yu, *Phys. Rev. E*, to be published.
- [13] M. Ota and T. Miyamoto, *J. Appl. Phys.* **76**, 5528 (1994).

FIGURES

FIG. 1. Comparison of multiple image results with Klingenberg's force functions.

FIG. 2. Force for longitudinal field: (a) $\beta=9/11$, (b) $\beta=1/3$.

FIG. 3. Comparison between analytic and simulation results in athermal aggregation: (a) uniaxial field, (b) rotating field.

FIG. 4. Displacement-time graph for athermal aggregation of two spheres in uniaxial field.

FIG. 5. Reduction of aggregation time for: (a) uniaxial field, (b) rotating field.

FIG. 6. Displacement-time graph for athermal aggregation of two spheres in rotating field.

FIG. 7. Reduction of aggregation time for three and four spheres in rotating field.

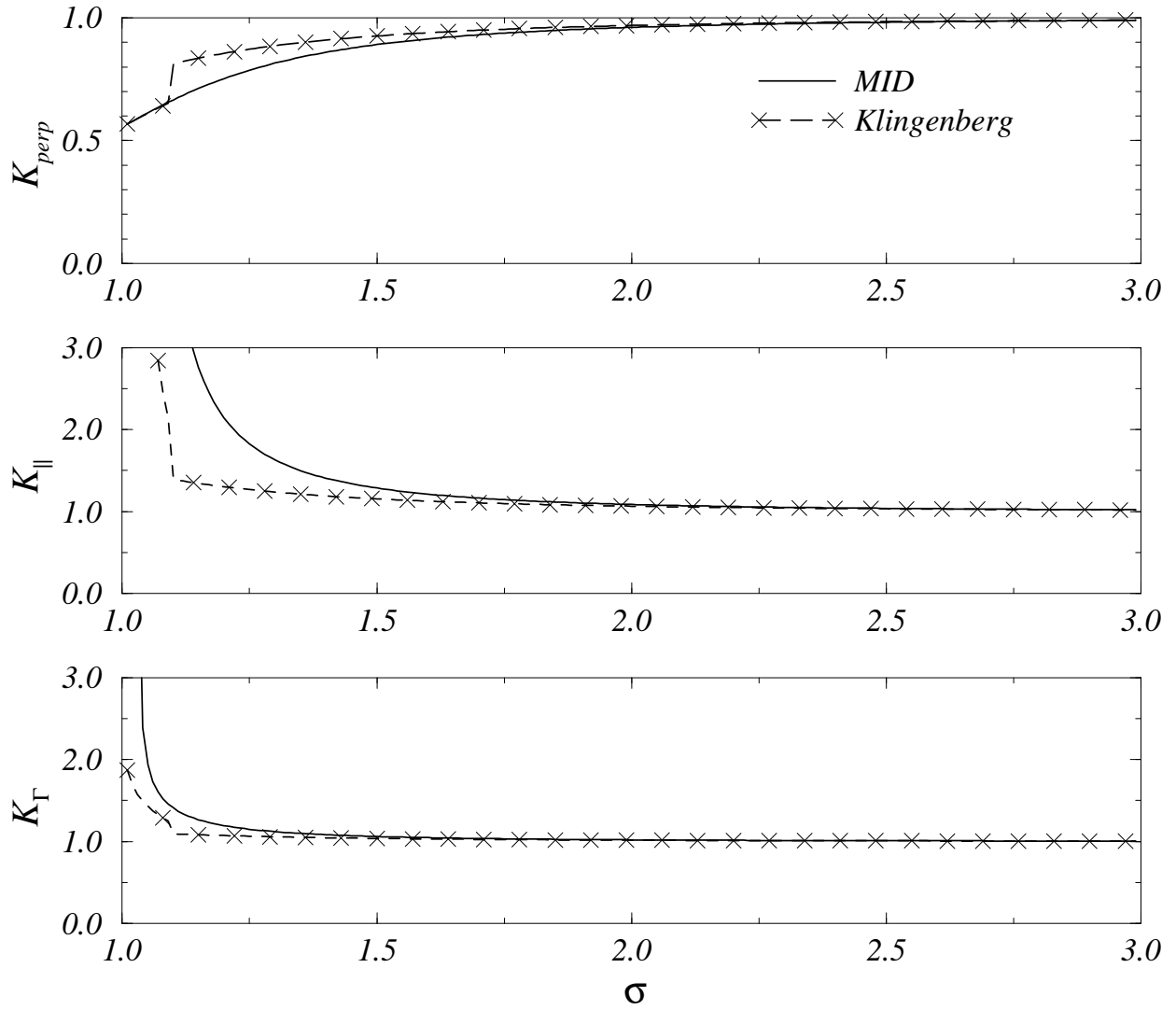


Fig.1

(a) $\beta = 9/11$

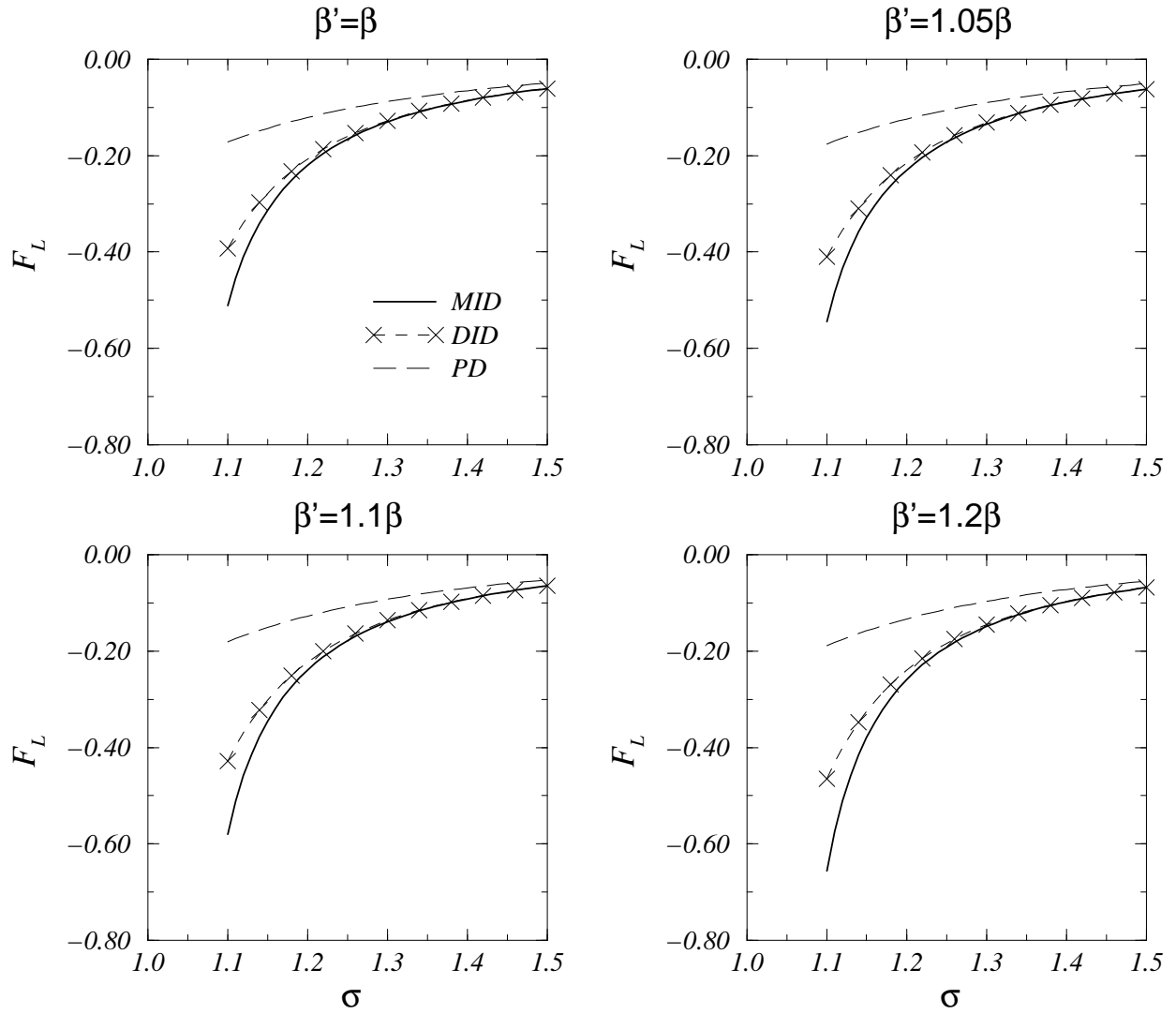


Fig.2(a)

(b) $\beta = 1/3$

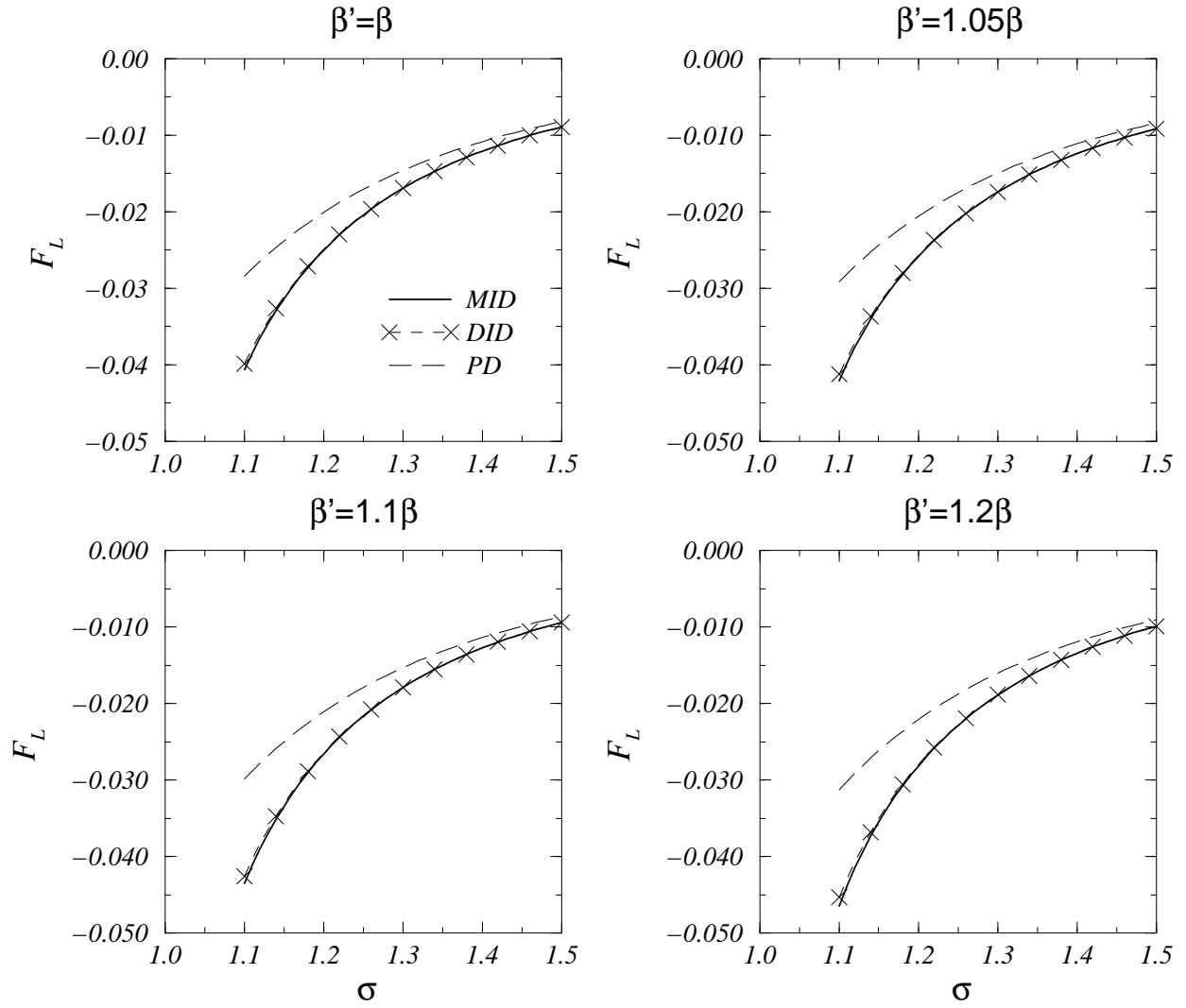


Fig.2(b)

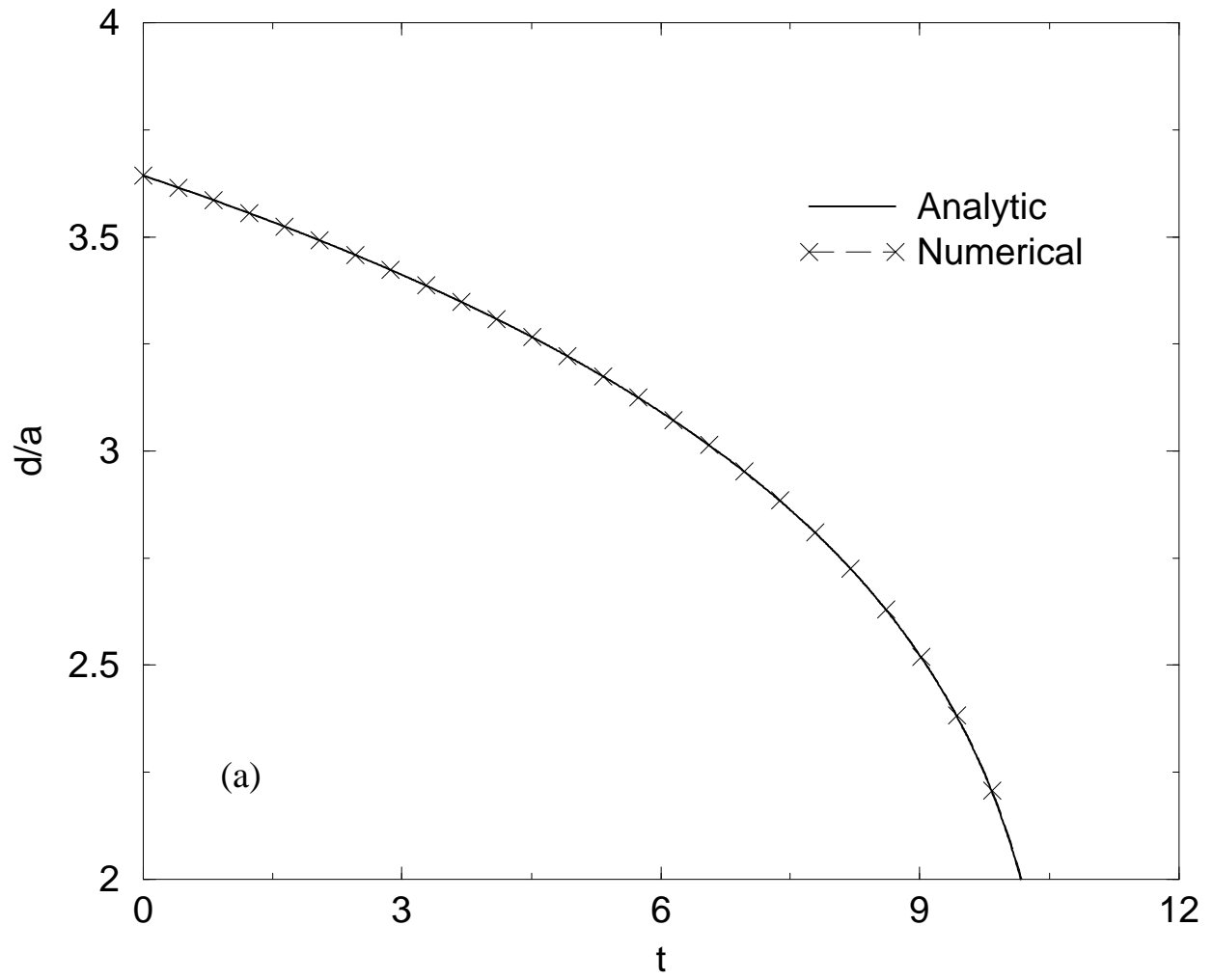


Fig.3(a)

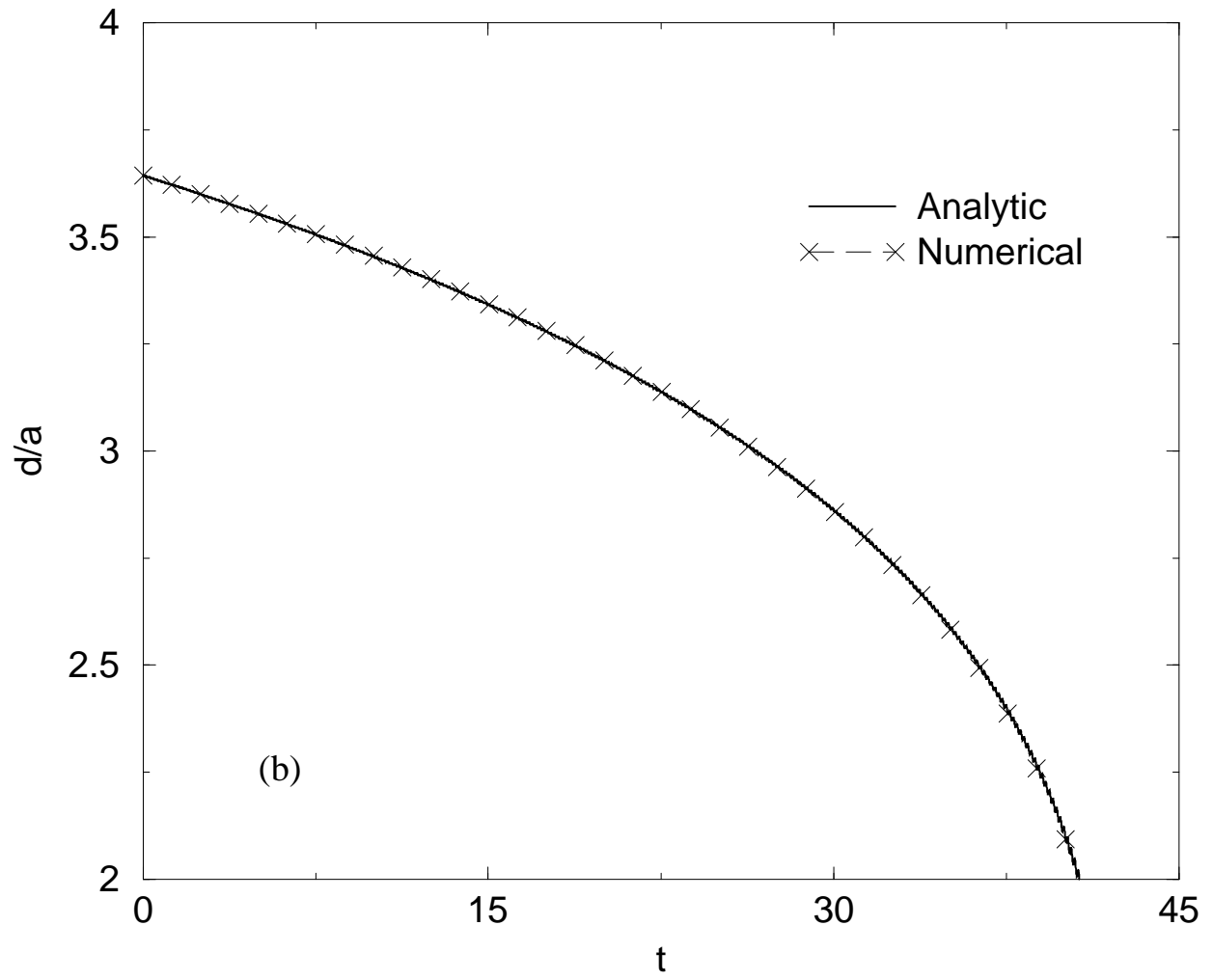


Fig.3(b)

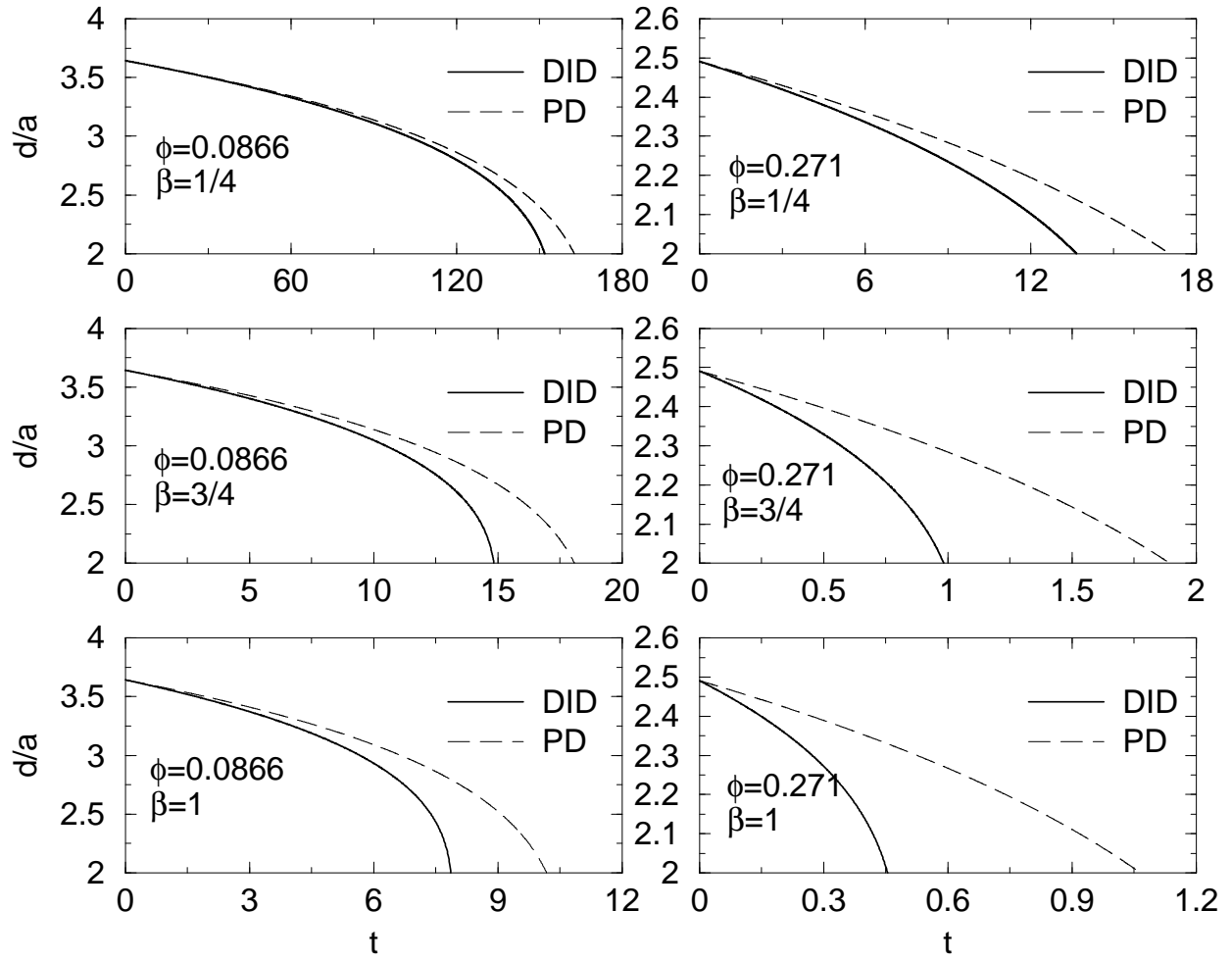


Fig.4

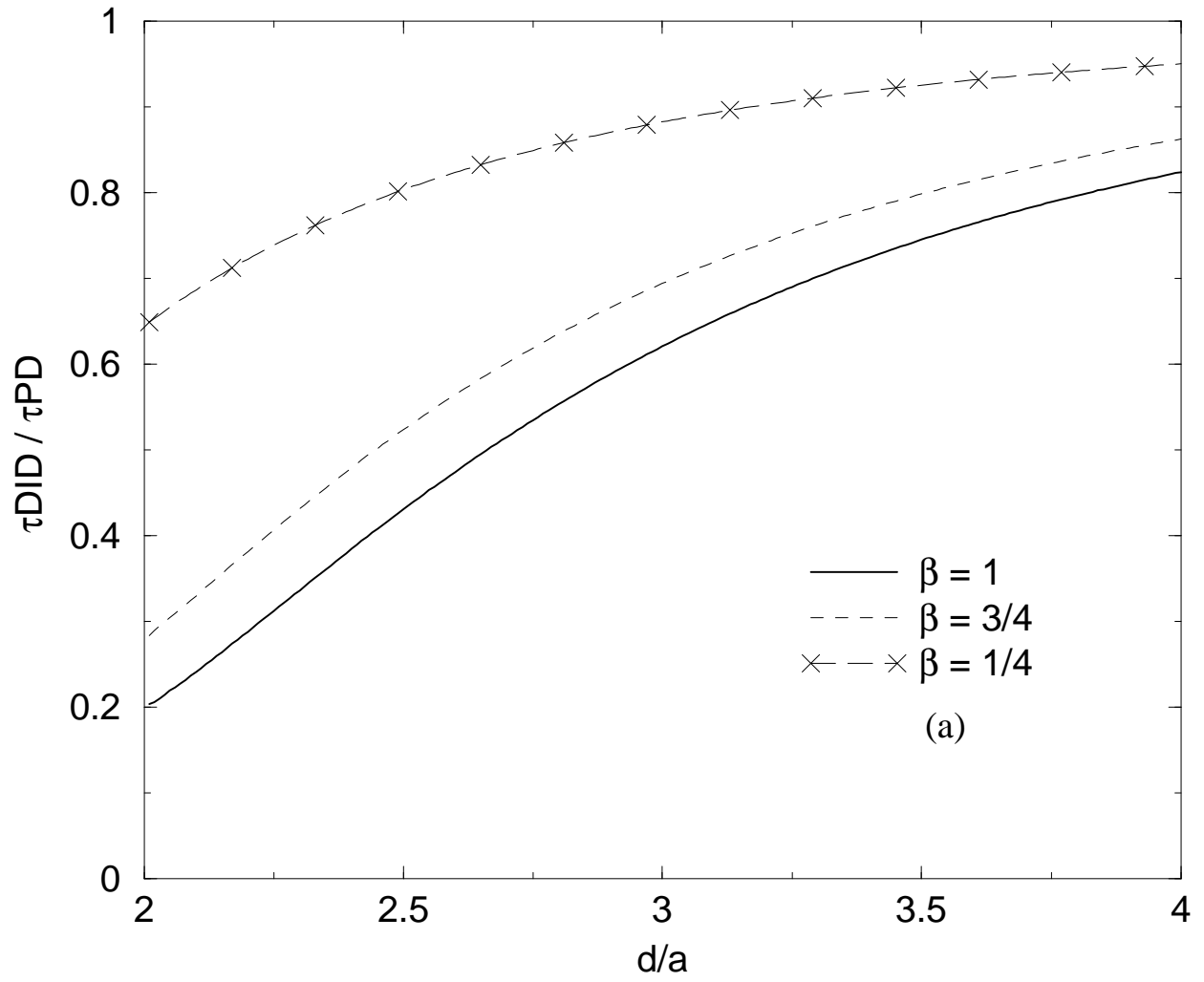


Fig.5(a)

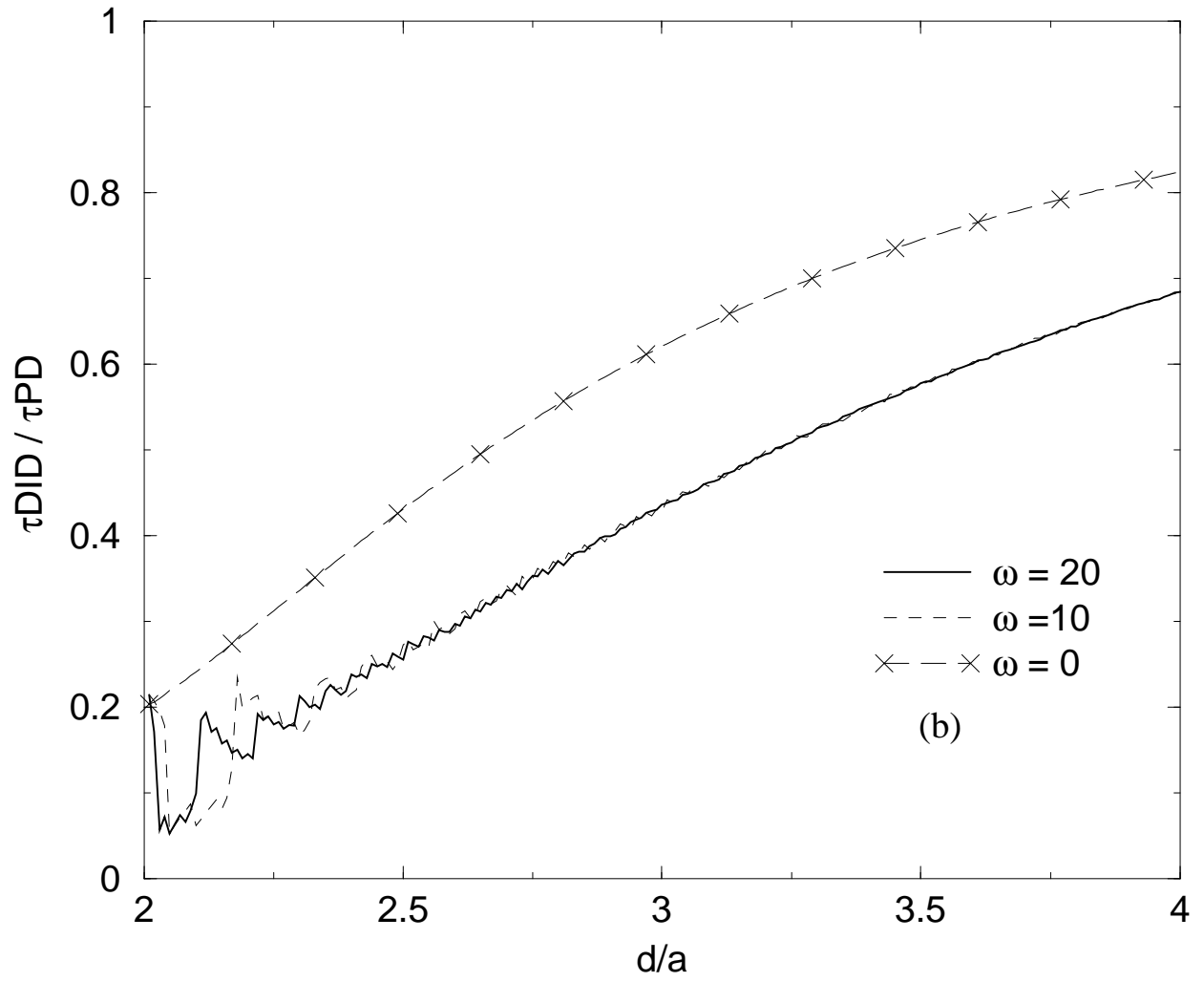


Fig.5(b)

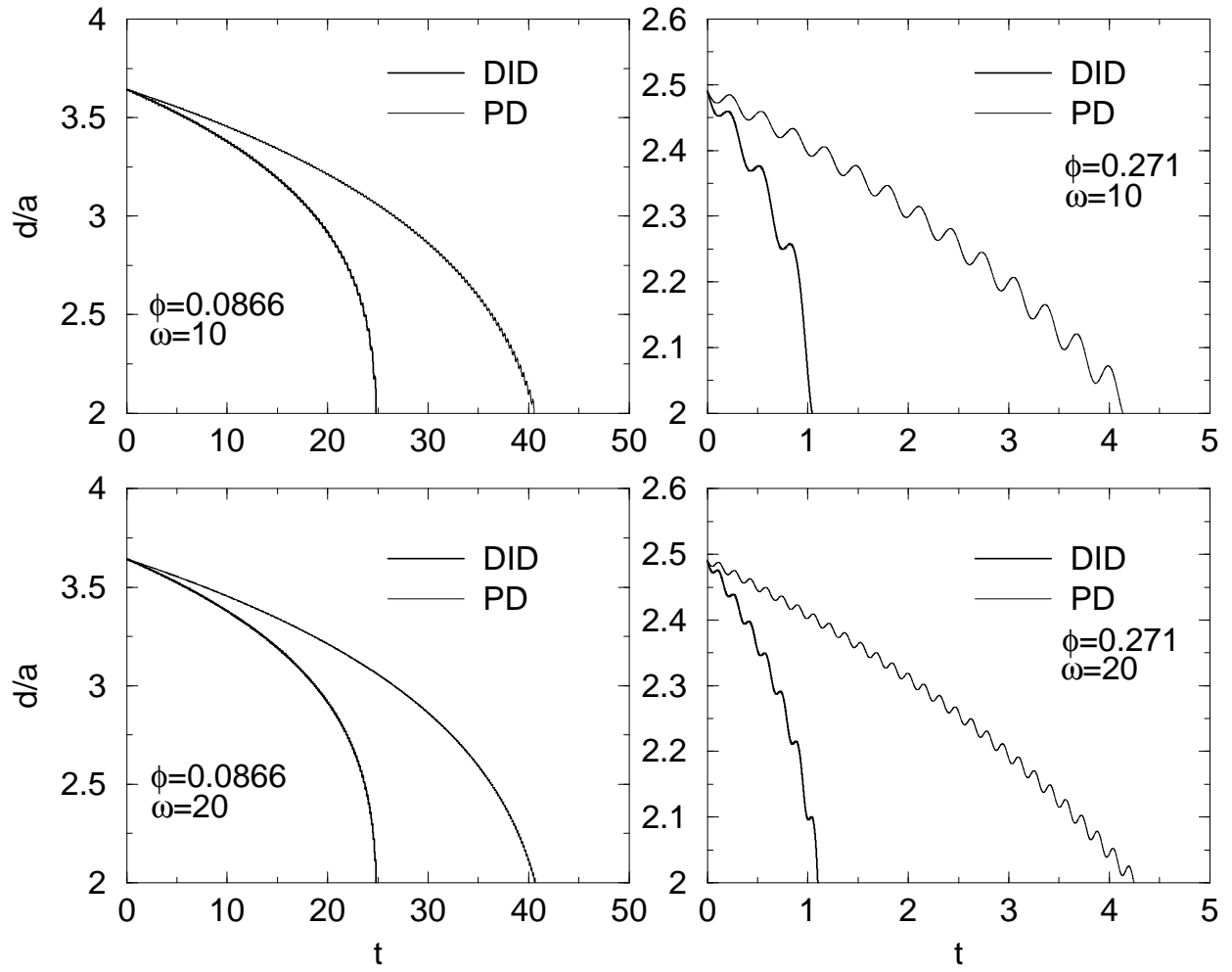


Fig.6

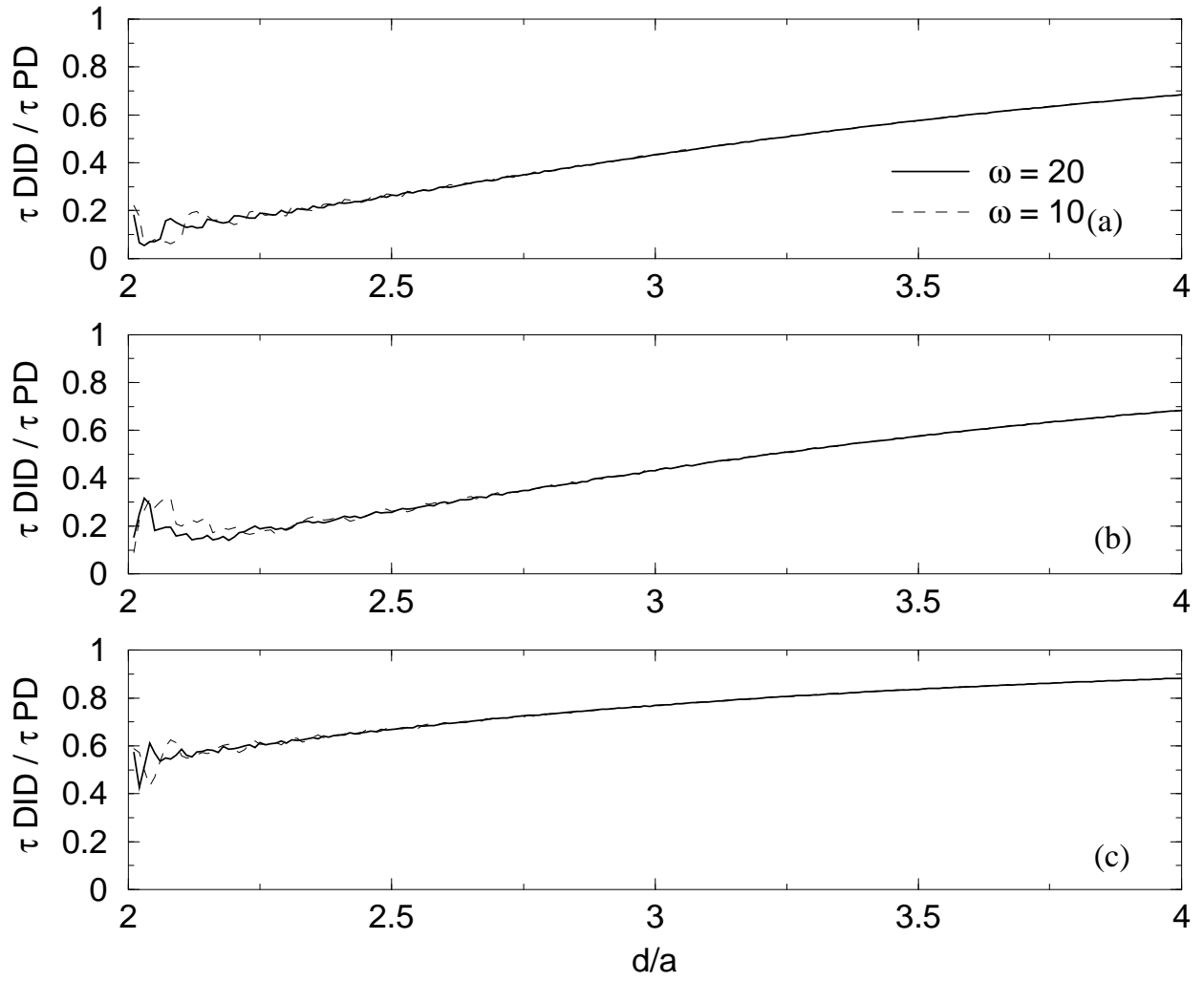


Fig.7